

Article

Characterisation of the Hydrogeological Properties of the Ntane Sandstone Aquifer Using Co-Seismic and Post-Seismic Groundwater Level Responses to the Mw 6.5 Moiyabana Earthquake, Central Botswana

Tshepang Mmamorena Marema^{1,2}, Loago Molwalefhe¹ and Elisha M. Shemang^{1,*}

¹ Department of Earth and Environmental Sciences, Faculty of Science, Botswana International University of Science and Technology, Private Bag 16, Palapye 10071, Botswana;

tshepang.marema@studentmail.biust.ac.bw (T.M.M.); molwalefhel@biust.ac.bw (L.M.)

² Aqualogic (Pty) Ltd., Plot 140, Unit 3, Kgale Terrace, Gaborone P.O. Box 403975, Botswana

* Correspondence: shemange@biust.ac.bw

Abstract: The 3 April 2017 Mw 6.5 Moiyabana earthquake (Central Botswana) had a significant impact on groundwater levels; a gradual co-seismic increase and a stepwise decline in groundwater levels were observed in response to the earthquake at boreholes MH2 and Z12836, respectively. In this study, we investigated the response of groundwater levels to Earth tides by computing the amplitude and phase shift of the M_2 tidal constituent to estimate the temporal variations of the storativity, transmissivity, and permeability of the Ntane sandstone aquifer (the main aquifer system) prior to and after the earthquake event. The storativity and permeability computed for borehole MH2 showed a decrease in magnitude of 3.17432×10^{-4} and $1.85 \times 10^{-13} \text{ m}^2$ respectively, indicating that strong ground shaking at borehole MH2 might have consolidated the aquifer material, thus resulting in decreased aquifer permeability. The aquifer coefficient of storativity decreased by 2.85×10^{-4} while permeability was enhanced by $0.047 \times 10^{-13} \text{ m}^2$ at borehole Z12836. Enhanced permeability might have resulted from increased/enhanced fracturing of the aquifer, fracture clearing and dynamic shaking.

Keywords: co-seismic groundwater level changes; Moiyabana earthquake; Characterisation; hydrogeological properties; post-seismic groundwater level changes



Citation: Marema, T.M.; Molwalefhe, L.; Shemang, E.M. Characterisation of the Hydrogeological Properties of the Ntane Sandstone Aquifer Using Co-Seismic and Post-Seismic Groundwater Level Responses to the Mw 6.5 Moiyabana Earthquake, Central Botswana. *Water* **2023**, *15*, 1947. <https://doi.org/10.3390/w15101947>

Academic Editors: Galina Kopylova and Svetlana Boldina

Received: 13 April 2023

Revised: 14 May 2023

Accepted: 18 May 2023

Published: 21 May 2023



Copyright: © 2023 by the authors. Licensee MDPI, Basel, Switzerland. This article is an open access article distributed under the terms and conditions of the Creative Commons Attribution (CC BY) license (<https://creativecommons.org/licenses/by/4.0/>).

1. Introduction

Aquifers are responsive to external stresses and periodic loadings such as atmospheric pressure variations, Earth tides and seismic waves [1–4]. Changes in groundwater levels in confined aquifers occur in response to Earth tides and atmospheric pressure loads [1,5–8]. Variabilities in well levels caused by earthquakes have been measured and widely studied [4,9–12]. These variations are sufficiently large to be measured and recorded, and their analysis is very useful in determining the elastic properties and porosity of aquifers [1,13].

Borehole hydrographs are analysed following an earthquake event to identify pre-seismic, co-seismic, and post-seismic groundwater level changes and the observed changes are used to investigate temporal changes in the aquifer's hydraulic properties [11]. Co-seismic groundwater level responses may vary depending on factors such as the earthquake magnitude, distance from the earthquake epicenter, the magnitude of the seismic energy density, hydrogeological properties of the aquifer system and well construction and design [3,11,14]. Earthquake-induced groundwater level changes thus manifest as abrupt step-like changes (rises or falls) in the near-field, gradual changes in the intermediate field and oscillations in the far-field [4–6].

Earthquakes can modify aquifer properties and the observed changes in groundwater level may reflect the equilibration of these properties [7]. The passage of seismic waves through aquifers also contributes to changes in the permeability of the well-aquifer system. When the change in the permeability is not reversed after the seismic waves propagate through the aquifer system, there would be major differences in the groundwater levels before and after an earthquake [8]. The change in transmissivity and storage coefficient induced by earthquakes can cause variations in the phase shift and amplitude of different tidal wave constituents [9]. Thus, the groundwater level tidal response reflects the aquifer properties [8,10,11].

Aquifer parameters, such as specific storage and transmissivity, can be derived from the response of groundwater levels to Earth tides [9,12,13]. The amplitude response of the tides is primarily related to the elastic properties and the porosity of the aquifer [12,14]. However, the phase lag between the tidal dilation of the aquifer and the groundwater-level response in wells is mainly affected by the aquifer's transmissivity and storage coefficient [15]. Therefore, the computed amplitude response and phase shift tidal response are used to monitor the storativity and transmissivity of an aquifer before and after the earthquake, respectively [2,9].

Mechanisms that account for co-seismic groundwater level changes include (1) enhancement of the aquifer's permeability, (2) co-seismic liquidation or consolidation of loose sediments and (3) co-seismic static strain and changes in the pore pressure [7,8,16,17]. Analyses of the groundwater level tidal response in wells have confirmed that large earthquakes tend to change the permeability of aquifers locally [8,18–20]. Permeability is effectively enhanced through development of new fractures in the aquifer and clearing of mineralised fractures during dynamic shaking of the existing fracture system [8]. However, the increased permeability will eventually decrease over time due to hydrogeological and/or biogeochemical processes that re-clog the fractures [7]. Sustained co-seismic groundwater level changes are attributed to the redistribution of stress and strain due to opening of fractures during earthquakes [3]. Sustained co-seismic groundwater level drop may indicate changes in the poroelastic property of the aquifer system [21].

The 3 April 2017 Mw 6.5 Moiyabana earthquake was the second largest earthquake recorded since monitoring began in Botswana [22–25]. The earthquake induced distinct co-seismic groundwater level responses in a nearby borehole MH2 and a distant borehole Z12836, which are located 40 km and 167 km from the epicentre, respectively. This earthquake event provided an opportunity to study the post-earthquake hydrogeological responses in the boreholes using time series data of the groundwater level monitoring in the area.

Problem Statement

Research directed at analysing the causative mechanism of the Moiyabana earthquake has received a lot of attention e.g., [22,23,26–29]. The interest was triggered by the earthquake's occurrence in an area considered part of a non-seismically active region [22,27,28]. There is, however, a notable lack of research on the effect of this earthquake on the groundwater resources of the nearby and regional aquifer (Ntane Sandstone aquifers). The current research is therefore directed at analysing effects of the earthquake on groundwater resources in the nearby and regional aquifer (Ntane Sandstone aquifer) This is important because large earthquakes can cause significant changes in the hydraulic properties of aquifers and aquitards, with far-reaching implications on the groundwater resources of the affected areas [20]. The Ntane sandstone aquifer covers large areas of central and eastern Botswana and is the main source of water to meet the water demands for domestic and industrial usage across many villages and towns in the area. It is therefore critical to investigate the impact of the earthquake on the hydraulic properties and water resources of the Ntane sandstone aquifer.

The objectives of this study were to analyse the borehole hydrographs for pre-seismic, co-seismic and post-seismic groundwater level responses to the Moiyabana (Mw 6.5)

earthquake and to compute the tidal amplitude and phase shift of the M_2 tidal constituent to estimate the aquifer's storativity, transmissivity and permeability prior and following the earthquake.

2. Materials and Methods

2.1. Study Location

The CIC Energy Wellfield (referred to as the Kudumatse area) is a 150 km² wellfield situated to the southwest of Kudumatse village in-southeast Botswana. The borehole Z12836 (23.510° S and 26.699° E) located in this wellfield is approximately 167 km from the Moiyabana earthquake's epicentre (Figure 1).

The Gope Well field (referred to as the Gope area) covers an area of approximately 45 km² within the Central "Kalahari Game Reserve (CKGR)". The wellfield belongs to the Ghaghoo Diamond Mine, formerly known as Gope Mine. The remotely located Ghaghoo Diamond mine is approximately 45 km west of the eastern border of the CKGR. It is within this wellfield that borehole MH2 (22.626° S and 24.762° E) is located approximately 40 km from the Moiyabana earthquake's epicentre (Figure 1).

The two wellfields are part of the Central Kalahari Basin (CKB) which is predominantly filled by Karoo age sediments that are covered by flat terrain of the younger Aeolian sands of the Kalahari Group [30–32]. The CKB is characterized by a semi-arid to arid climate with characteristic cold, dry winters and hot wet summers [32]. Rainfall is highly variable in the CKB area, both spatially and temporally [33]. Nearly all rainfall occurs as convective thunderstorms during the summer season between September and April, with an average of about 380–530 mm/annum [32].

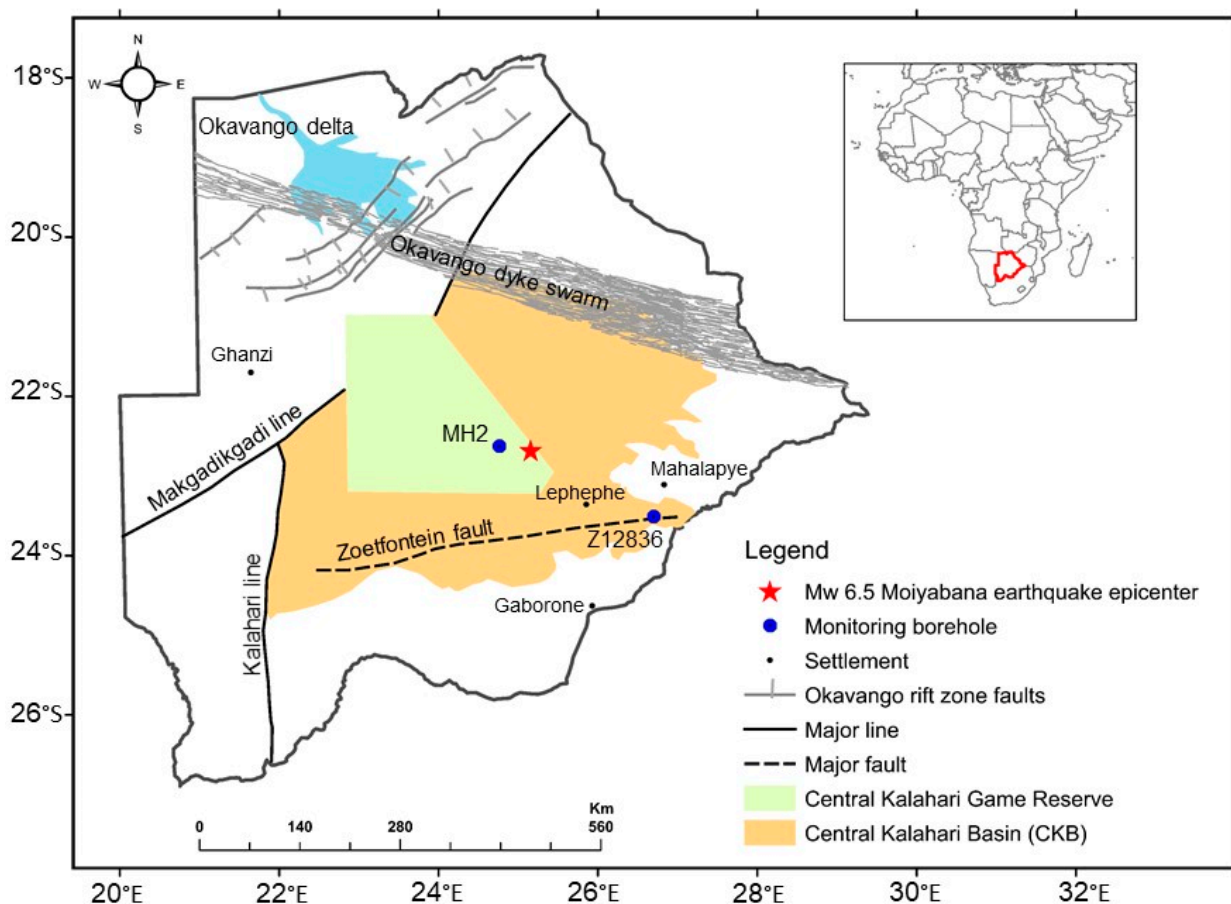


Figure 1. Map of Botswana showing the Central Kalahari Basin and the major structures associated with it and the location of borehole MH2 and Z12836 (modified from [23,32,34]).

2.1.1. Geology

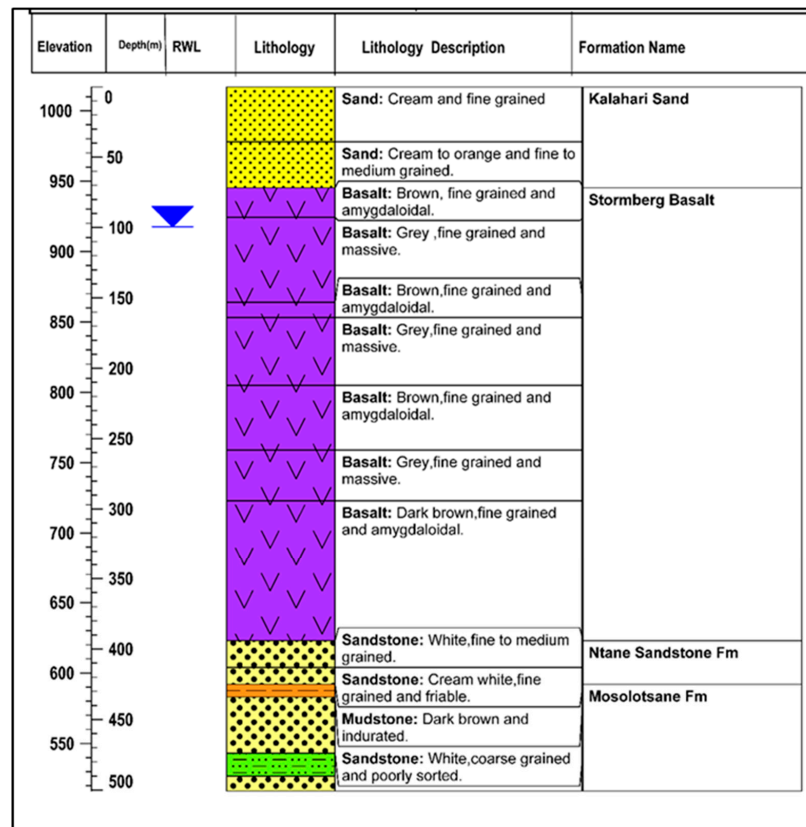
The CKB area is underlain by the Carboniferous to Jurassic age sedimentary succession of the Karoo Supergroup. The Karoo unconformably overlies the Archaean basement and Proterozoic rocks [31,33–35]. The Archaean basement consists of granitic gneisses of varying compositions, metasediments and the amphibolite to the Limpopo-Shashe Belt [36,37]. The Karoo Supergroup succession is capped by widespread continental flood basalts of the Stormberg Basalts [38]. Younger Tertiary to Quaternary Kalahari sands overlie the CKB rocks and the bedrock geology [31,34,35]. The CKB boundaries have been defined by the E–W-trending Zoetfontein Fault, Limpopo Mobile Belt, Okavango Dyke Swarm to the North and the N–S-trending Kalahari Line to the western edge of the Kaapvaal Craton and the NE–SW-trending Makgadikgadi Line that defines the north-western edge of the Zimbabwe Craton [30,33,39].

Pre-Karoo igneous intrusions that include dolerite dikes and inclined sills have been mapped in the study area [31,32]. The ENE–WSW regional Zoetfontein fault (Figure 1) formed in the Lower Proterozoic age is the most prominent structure. The intrusions emanate from this fault zone along with other conjugate structures due to frequent lateral movement [32,34,40]. Post-Karoo dolerite dykes, sills and diamondiferous kimberlite intruded the Karoo rocks along a WNW–ESE trend [34]. The Zoetfontein Fault was affected by the NW-to-NNW- and NE-trending post-Karoo normal faults [32]. Several faults that trend in the NNW–SSE, ENE–WSW and WNW–ESE orientations transect the Zoetfontein fault, indicating that they post-date it [31,32]. A majority of the faults in the area are younger or the same age as the Stormberg Basalt, as they cut through the entire stratigraphic sequence except for the Kalahari Sand [40–43]. These normal faults have created a complex set of horst and graben structures [32].

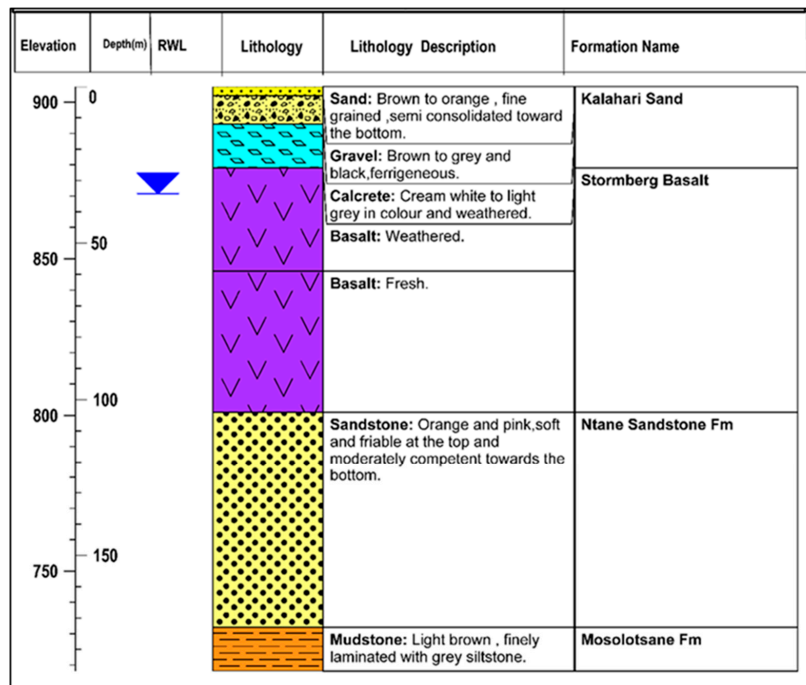
2.1.2. Hydrogeology and Aquifer Parameters

Groundwater in the study area has been limited to the Stormberg basalt, Ntane sandstone and sedimentary sequences of the Ecca Group [30]. The most productive and prominent aquifer in the study area is the Ntane aquifer (comprised of fine-medium-grained sandstone). The Ntane Sandstone aquifer is a dual-porosity aquifer, with the interstitial porosity associated with the poorly cemented Ntane Sandstone Formation and the secondary porosity associated with post-Karoo lineaments that cut through the Karoo lithologies [40].

Lineaments in the Ntane sandstone provide additional pathways for water movement, with the matrix inherently providing matrix storage potential especially where the Ntane sandstone is weathered [40]. The Ntane sandstone aquifer has high transmissivity values where fracturing is well developed and cementation is less, hence the Ntane sandstone's high porosity and permeability are attributed largely to intense fracturing [33]. The Ntane sandstone aquifer is confined at the top by the basalt cap and below by the low permeability mudstone and siltstone of the Mosolotsane Formation (Figure 2a,b). Where the Stormberg basalt cap is missing or completely eroded, the Ntane sandstone is hydraulically connected with the overlying Kalahari Sands and thus constitutes an unconfined aquifer [40]. The regional groundwater rest levels are approximately 100 m and 34 m in the Gope and Kudumatse areas respectively, indicating confined aquifer conditions [41–43].



(a)



(b)

Figure 2. (a) Lithological log and description of borehole MH2 located in the Gope wellfield, indicating the position of the Ntane sandstone aquifer, the lower confining mudstones and the volcanic cap [44]; (b) Lithological log and descriptions of borehole Z12836 in the CIC Energy wellfield indicating the position of the Ntane sandstone aquifer, the lower confining mudstones and the volcanic cap [43].

The hydraulic conductivity (K), transmissivity (T) and Storativity (S) of the Ntane aquifer were calculated using the Cooper-Jacob (1946) technique under a constant-rate pumping test [44]. The results are as follows; for borehole MH2, $K = 0.098$ m/day, $T = 6.822$ m²/day and $S = 0.0001$, and for borehole Z12836, $K = 0.488$ m/day $T = 33.696$ m²/day and $S = 0.0002$ [41–43]. These storativity values are indicative of confined aquifer conditions. The Kudumatse area is considered a high transmissivity zone, with T ranging from 500–3300 m²/day, and this is attributable to heavy fracturing and the low cementation of the sandstone [42].

2.1.3. Borehole Construction

Neither of the boreholes were screened, and thus the steel casing installed in the boreholes was perforated at the aquifer interval to allow the ingress of groundwater into the borehole. The steel casing for borehole Z12836 had a diameter of 254 mm and 203 mm from intervals 0–17 mbgl and 1 to 187 mbgl, respectively. The wellbore is open at 104–173 mbgl at Ntane sandstone, which is the principal aquifer. The perforated casing length is 69 m. It should be noted that the Ntane sandstone is friable towards the top of the stratigraphic succession, and it becomes moderately competent towards the bottom.

The casing diameter for borehole MH2 for example was 203 mm. The wellbore is open at 394–425 mbgl at Ntane sandstone aquifer, which is the main water bearing rock (Table 1). Therefore, the perforated casing length is 31 m and the borehole drilling diameter was 254 mm.

Table 1. Summary of the hydrogeological conditions at boreholes MH2 and Z12836.

Borehole ID	Borehole Depth (mbgl)	Depth to Base (mbgl)				Water Strike (mbgl)	Rest Water Level (mbgl)
		Kalahari Beds	Stormberg Basalt	Ntane Sandstone Fm	Mosolotsane Fm		
MH2	501	71.8	394	425	>501	211; 388	99.362
Z12836	187	26	104	173	>187	58; 104; 112	34.19

2.2. Methodology

2.2.1. Sampling

Groundwater level was recorded at a temporal resolution of 6 h at boreholes Z12836 and MH2. Barometric pressure was measured for borehole BH7435 at a temporal resolution of 12 h using the Baro-Diver data logger, which recorded the semi-diurnal atmospheric pressure variations. Borehole BH 7435 is situated 25 km from borehole Z12836. The groundwater level and barometric pressure measurements were recorded during the period of February 2016 to March 2018 at borehole Z12836, while at borehole MH2, the groundwater level was recorded from January 2016 to December 2018.

2.2.2. Borehole Hydrograph Analysis

Borehole hydrographs were analysed to identify the pre-, co- and post-seismic groundwater level responses due to the Moiyabana earthquake. Earthquake-induced groundwater level changes can be detected by analysing anomalous signals of groundwater level time series information from a monitoring well, in order to detect earthquake-induced groundwater level changes [1]. Co-seismic groundwater level changes manifest themselves as step-like changes, gradual changes and oscillations [5,45]. Post-seismic water level adjustment or recovery is termed ‘post-seismic groundwater recession’ [4,46].

2.2.3. Tidal Analysis

After all the data were resampled into hourly measurements, we applied a least-squares method for tidal analyses using the Tsoft software program, Version 2.2 [9,47]. Spectral analysis was performed on the MH2 and Z12836 groundwater levels, and the

barometric pressure time series data were used to identify periodic fluctuations in the data and to extract the dominant tidal components using the Tsoft software package [47]. Tsoft uses a Fast Fourier Transformation (FFT) algorithm to calculate time series data spectra [48,49].

A low-pass filter and a high-pass Butterworth filter with a cut-off frequency equal to 3.0 cpd and 0.8 cpd (cycles per day) respectively were applied to the groundwater level data to enhance the signal-to noise ratio of the main tidal constituents [10,50]. In this study, barometric loading was extracted from the groundwater level data using the Bayesian Tidal Analysis Program (Baytap-G) software, Version 1.9.2 developed in [51]. This was achieved using the non-harmonic method based on multiple linear regression [52]. Borehole MH2 had no barometric pressure record; therefore no barometric pressure correction was performed on the groundwater levels data. The impact of the lack of barometric pressure record on the M_2 tidal component of the groundwater level for borehole MH2 is likely to have minimal impact on the M_2 component of the groundwater level [9,21]. Moreover, since borehole MH2 and Z12836 are far from the coastline, ocean tide corrections were also deemed not very necessary [21].

The main tidal wave components that have a significant effect on groundwater level variations are O_1 , M_2 , N_2 , K_1 and S_2 waves, Table 2 [2,6,53]. Tidal waves greater in amplitude of the five major tidal components, i.e., M_2 and O_1 , are usually preferred to evaluate the groundwater-level response to earth tides because they have a greater signal-to-noise ratio [6,9,49]. However, in this study, only the lunar semi-diurnal (M_2) wave constituent was used to estimate the aquifer hydraulic properties. This is because it is more stable, exhibits a large amplitude and the smallest root-mean-square error, and is less affected by external influences from solar radiation/thermal effect and diurnal barometric pressure effects than the O_1 tidal component [2,9–11,21,46,49].

Table 2. Major harmonic components of the tidal potential (adapted with permission from Munk & MacDonald [53], 1960, Munk & MacDonald).

Tidal Component	Description	Period (Day)	Frequency, cpd (Cycles per Day)
O_1	Principal lunar	1.0758	0.9295
K_1	Lunar-solar	1.3721	1.0029
N_2	Lunar elliptic	0.5275	1.8957
M_2	Principal lunar	0.5175	1.9324
S_2	Principal solar	0.5000	2.0000

A window size of 31 days was chosen for this study to separate the time domain tidal analysis for the semidiurnal M_2 and the diurnal S_2 tidal components and to avoid spectral leakage [10,54,55]. Thus, the response of groundwater level to the volumetric strain associated with the M_2 tidal constituent was obtained every 31 days using the Baytap-G software. The pre-earthquake period was taken as 31 days before the earthquake and 31 days after the earthquake for the post-earthquake period, allowing for a comparison to be made, and also to be determine the impact of the Moiyabana earthquake on the hydraulic properties of the aquifer. In order to estimate earthquake-induced changes in the hydraulic properties of the Ntane sandstone aquifer system, the groundwater level response to earth tides and atmospheric pressure before and after the Moiyabana earthquake's occurrence were used.

2.3. Mechanisms for Classifying/Determining the Hydrogeological Properties

2.3.1. Estimating the Aquifer Storage Coefficient

The variation in groundwater level produced by aquifer dilatation as a result of Earth tide is a function of the aquifer's specific storage and can be calculated by measuring fluctuations in groundwater level (dh) and tidal component amplitude [9]. The storage coefficient S is the product of the aquifer specific storage S_s and the thickness of the aquifer,

d. The specific storage S_s therefore can be calculated from the groundwater level tidal-response amplitude [6,56,57] using Equation (1). The minus sign in Equation (1) indicates that the tide-generating potential increases when the head in the aquifer decreases [57].

$$S_s = \left\{ \left[\left(\frac{1 - 2\nu}{1 - \nu} \right) \left(\frac{2\bar{h} - 6\bar{l}}{a} \right) \right] \frac{dW_2}{g} \right\} (-dh^{-1}) \tag{1}$$

where ν is the Poisson ratio, \bar{h} is the love number of the surface of the earth (0.60), \bar{l} is the love number at surface of the earth (0.07) [53], a is the mean earth radius 6.371×10^8 cm and W_2 is the theoretical tidal potential $W_2 \approx A_2(\theta, \delta) = gK_m b f(\theta)$ [57]. The terms enclosed in the brackets will always be constant for general aquifer materials i.e., 7.88×10^{-9} , hence:

$$S_s = 7.880 \times 10^{-9} \cdot \frac{A_{2(\tau, \theta)}}{A_h(\tau)} \tag{2}$$

where is $A_h(\tau)$ the fluctuation amplitude induced by the different tidal period components; $A_{2(\tau, \theta)}$ is the fluctuation amplitude of the second-step tide-generating potential; K_m is the general lunar coefficient, typically taking a value of ~ 0.537 m [53]; b is a constant related to the period of the various tidal wave component or the amplitude factor for various tidal components; and $f(\theta)$ is a function of latitude θ or the latitude dependence factor. For the semi-diurnal M_2 wave, $f(\theta) = 0.5\cos^2(\theta)$ and $b \approx 0.908$ [53,57].

After obtaining the specific storage S_s using Equation (2), the storage coefficient S can be calculated using $S = S_s \times d$. d is the thickness of the aquifer.

2.3.2. Estimation of the Aquifer Transmissivity Using Phase Shift The Horizontal Flow Model

The Hsieh solution [9] was used to calculate the transmissivity of an aquifer when the phase shift of the groundwater level relative to the tidal strain is negative i.e., ranging from -90° to -1° [58]. The Hsieh solution is used for the tidally induced radial flow of groundwater to a well (assuming a horizontal, laterally extensive, confined, isotropic and homogeneous aquifer that is fully penetrated by a well) to estimate the aquifer transmissivity from the phase shift associated with the M_2 tidal constituent. The Hsieh solution can be approximated for a realistic well geometry and aquifer properties as

$$s_w = \frac{Q_0}{2\pi T} \{ [\phi \text{Ker}(\alpha\omega) - \psi \text{Kei}(\alpha\omega)] + i[\psi \text{Ker}(\alpha\omega) + \phi \text{Kei}(\alpha\omega)] \} \tag{3}$$

With

$$\phi = \frac{-[\text{Ker}_1(\alpha\omega) + \text{Kei}_1(\alpha\omega)]}{2^{1/2}\alpha\omega [\text{Ker}_1^2(\alpha\omega) + \text{Kei}_1^2(\alpha\omega)]} \tag{4}$$

$$\psi = \frac{-[\text{Ker}_1(\alpha\omega) + \text{Kei}_1(\alpha\omega)]}{2^{1/2}\alpha\omega [\text{Ker}_1^2(\alpha\omega) + \text{Kei}_1^2(\alpha\omega)]} \tag{5}$$

$$\alpha\omega = (\omega S/T)^{1/2} \cdot r_w \tag{6}$$

$$\omega = 2\pi/\tau \tag{7}$$

s_w is the drawdown at the well, which is related to the water level in the well (x) and the pressure head in the aquifer (h) by $h - s_w = x$, Q_0 is the discharge of the aquifer at the well, $\text{Ker}(\alpha\omega)$ and $\text{Kei}(\alpha\omega)$ are the Kelvin functions of order zero and $\text{Ker}_1(\alpha\omega)$ and $\text{Kei}_1(\alpha\omega)$ are the Kelvin functions of order one. ω is the tidal fluctuation frequency of the tidal wave constituent, taking the value of τ to be $0.5175/d$ for the M_2 wave. r_w is the inner radius of the well casing. T and S are the transmissivity and storativity of the aquifer, respectively.

The relationship between aquifer properties and the amplitude ratio, which is the ratio of the amplitude of tide of the water level in a well to the amplitude of the fluctuating pressure head in the elastic aquifer responding to the tidal stress, can be obtained [9]. The amplitude response A and the phase shift η can be defined using Equations (8) and (9) respectively.

The amplitude response A is:

$$A = (E^2 + F^2)^{-1/2} \tag{8}$$

While the phase shift η is:

$$\eta = -\arctan^{-1}(F/E) \tag{9}$$

where E and F are defined as

$$E = 1 - \frac{\omega r_c^2}{2T} [\psi \text{Ker}(\alpha \omega) + \phi \text{Kei}(\alpha \omega)] \tag{10}$$

$$F = \frac{\omega r_c^2}{2T} [\phi \text{Ker}(\alpha \omega) - \psi \text{Kei}(\alpha \omega)] \tag{11}$$

r_c is the inner radius of screened or open portion of the well. For Earth tide analysis, realistic values of r_w , T and S, and the value of $\alpha \omega$ computed by Equation (6) will usually be small (<0.1). In this case, both $\text{Ker}_1(\alpha \omega)$ and $\text{Kei}_1(\alpha \omega)$ can be approximated by $-1/(2^{1/2} \alpha \omega)$. This leads to $\phi \approx 0$ and $\psi \approx 0$ and E and F can thus be approximated according to Equations (12) and (13) respectively as:

$$E \approx 1 - (\omega r_c^2 / 2T) \text{Kei}(\alpha_w) \tag{12}$$

$$F \approx (\omega r_c^2 / 2T) \text{Ker}(\alpha_w) \tag{13}$$

Using r_c of 0.1015 m for both boreholes, τ for the M_2 tidal constituent is 12.421 h (44,715.6 secs); the transmissivity was calculated using the observed phase shift taking the well-aquifer parameter $Sr_w^2/r_c^2 = 1 \times 10^{-4}$ or negative phase shift as illustrated in [9].

Vertical Flow Model

The vertical flow model is used to estimate the transmissivity of an aquifer when the computed phase shift is positive. The vertical flow model ignores horizontal flow and predicts the phase shifts as positive (0–45°) between the groundwater level and the tidal strain [2,59]. The vertical flow model cannot cause negative phase lag beyond -1° . It is satisfied by undrained boundary conditions at an infinite depth and drained at the water table. Thus, the relationship between the groundwater level response inside a wellbore and the tidal fluctuations under these conditions can be estimated using Equations (14) and (15) [60].

The amplitude response A is defined as;

$$A = \left| \frac{x_0}{\varepsilon_0} \right| = \frac{1}{Ss} \left[1 - 2 \exp\left(-\frac{z}{\delta}\right) \cos\left(\frac{z}{\delta}\right) + \exp\left(-\frac{2z}{\delta}\right) \right]^{-1/2} \tag{14}$$

The phase shift η is defined as

$$\eta = \arg\left(\frac{x_0}{\varepsilon_0}\right) = \tan^{-1} \left\{ \frac{\exp(-\frac{z}{\delta}) \sin(\frac{z}{\delta})}{1 - \exp(-\frac{z}{\delta}) \cos(\frac{z}{\delta})} \right\} \tag{15}$$

The empirical variable is $\delta = \sqrt{2D/\omega}$, where D is the hydraulic diffusivity which is defined as the ratio of Transmissivity to Storativity and z is the depth from the surface to

the bottom of the borehole. Thus, the transmissivity of the aquifer can be estimated using the measured phase shift by Equation (16).

2.3.2.3. Estimation of the Aquifer's Permeability

The transmissivity T of an aquifer is estimated by following the standard method of fitting the tidal data for phase shift η using Equations (11) and (15), and using the measured values of r_c and r_w and the approximated value of S [8]. Then the estimated transmissivity is used to estimate the permeability of the aquifer. The relationship between T and permeability, k can be obtained using Equation (16) as follows:

$$k = \frac{\mu T}{b \rho g} \quad (16)$$

b denotes the thickness of the aquifer. ρ is the density, μ is the coefficient of dynamic viscosity of water, and g the gravitational acceleration and the typical values are 10^{-3} Pa·s, 10^3 kg/m³ and 9.81 m/s², respectively [61].

3. Results

3.1. Borehole Hydrograph Analysis

A gradual upward co-seismic groundwater level displacement of 1.565 m was observed in the hydrograph of borehole MH2 (Figure 3). This was followed by a post-seismic groundwater level recession. A full recovery to the pre-seismic groundwater levels was achieved after fifteen months (i.e., July 2018). The groundwater level recovery is also related to the permeability and thickness of the aquifer, with a thinner the aquifer, yielding a faster the rate of recovery of the co-seismic groundwater level change [3]. The recovery of the groundwater level to the pre-seismic groundwater level may show that re-equilibration of the aquifer properties occurred, which was changed by the earthquake's occurrence. Borehole MH2 is a dewatering borehole, as the mine is under care and maintenance. The anomalous rise at the end of the hydrograph might be indicating non-pumping periods, and therefore, recovery towards natural levels.

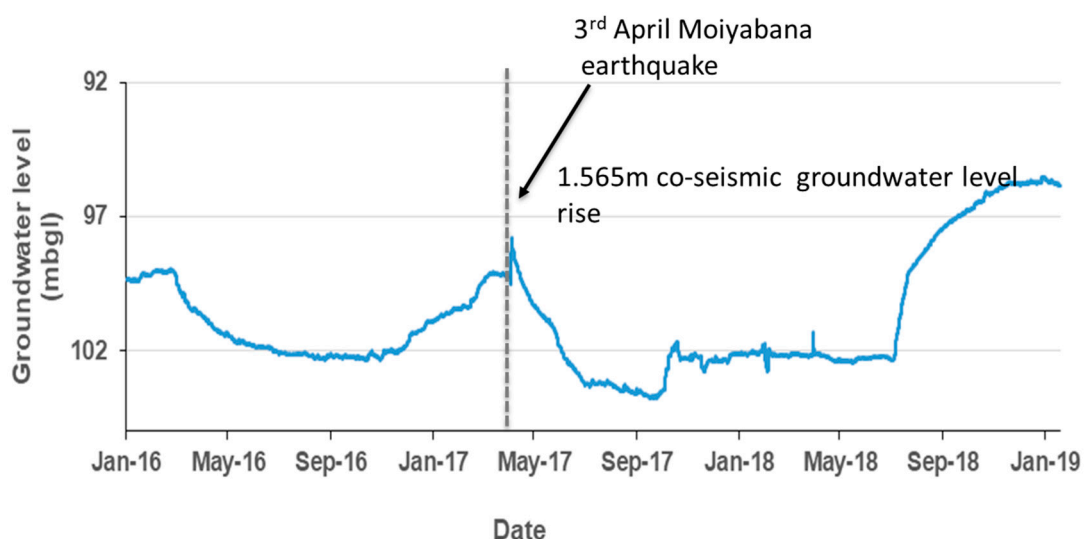


Figure 3. Borehole MH2 hydrograph showing the groundwater level variation during the period of monitoring.

A 0.2201 m co-seismic step-like fall in the groundwater level was observed in the hydrograph of borehole Z12836. Recovery to the pre-seismic groundwater level was not achieved in the period considered in this study (up to April 2018) (Figure 4). The co-seismic groundwater level was sustained in borehole Z12836, which might be an indication of a

permanent effect on the aquifer. As there was lack of groundwater level recovery observed at borehole Z12836 after the Mw 6.5 Moiyabana earthquake, this may be suggesting the occurrence of groundwater discharge, possibly through fractures generated by the earthquake [3,62]. As seismic shaking causes fracturing of the aquifer, the groundwater outflow through the fractures would further reduce pore pressure. Consequently, the aquifer can no longer return to the original state [3]. The earthquake triggered fractures might have created conduits through the confining layer to dissipate the pore pressure of the aquifer [3]. The confinement of the aquifer may also be breached by the fracturing due to seismic shaking during an earthquake. The dissipation of excess pressure in the confined aquifer generated by earthquakes is a slow process due to the retardation of the less permeable confining layer [3]. Therefore, groundwater level changes in confined aquifers are likely to be sustained for a long time.

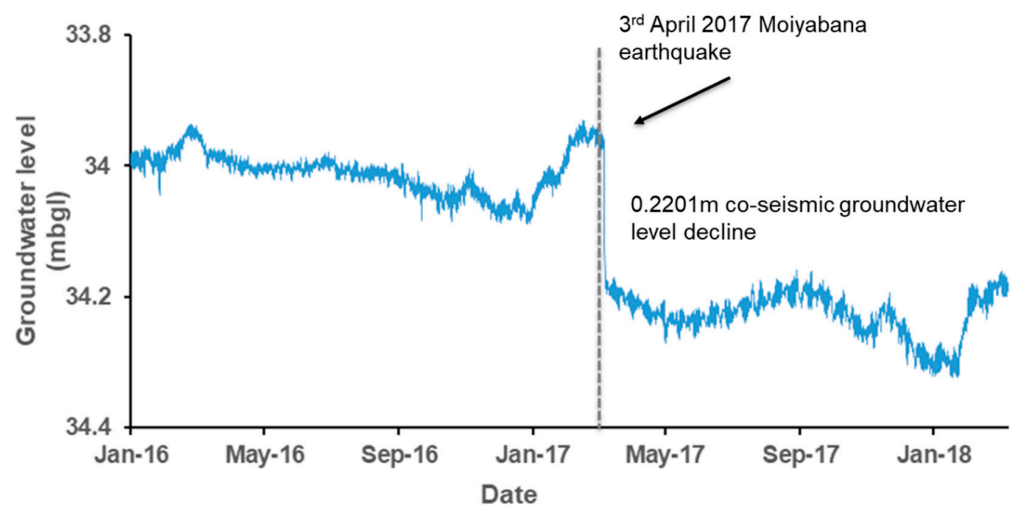


Figure 4. Borehole Z12826 hydrograph showing the groundwater level variation during the period of monitoring.

Seismic energy density in excess of 10^{-3} J/m^3 causes sustained groundwater level changes in wells. Seismic energy density is the maximum seismic energy required in a unit volume of rock or sediment to do work [4]. Thus, the seismic energy density $e \text{ (J/m}^3\text{)}$ is calculated according to the empirical relationship between earthquake magnitude (M_w) and earthquake epicentral distance $r \text{ (km)}$ [4] as follows:

$$\log r = 0.48M_w - 0.33\log e - 1.4 \tag{17}$$

The magnitude of the Moiyabana earthquake was $M_w 6.5$ and Table 3 indicates the epicentral distance used for the seismic energy density computations. The calculated seismic energy density values using Equation (17) for borehole MH2 and Z12836 are 2.277 J/m^3 and 0.0299 J/m^3 respectively (Table 3), which are within the range of seismic energy density capable of triggering sustained groundwater level changes induced by earthquakes; these values are also consistent with previous studies using global datasets [4,63]. Similarly, most sustained groundwater level changes are bounded by $e \times 10^{-3} \text{ J/m}^3$ [4].

Table 3. The computed seismic energy density experienced at the boreholes.

Borehole ID	Epicentral Distance (km)	Seismic Energy Density (J/m^3)
MH2	40	2.277
Z12836	167	0.0299

3.2. Spectra Analysis

The groundwater level spectra of the MH2 borehole show that the amplitude of the S_2 tidal component is greater than the M_2 tidal component (Figure 5). Therefore, because of this tidal component's low signal-to-noise ratio, the interpretation of the tidal response of the M_2 tidal component at borehole MH2 requires more caution [55].

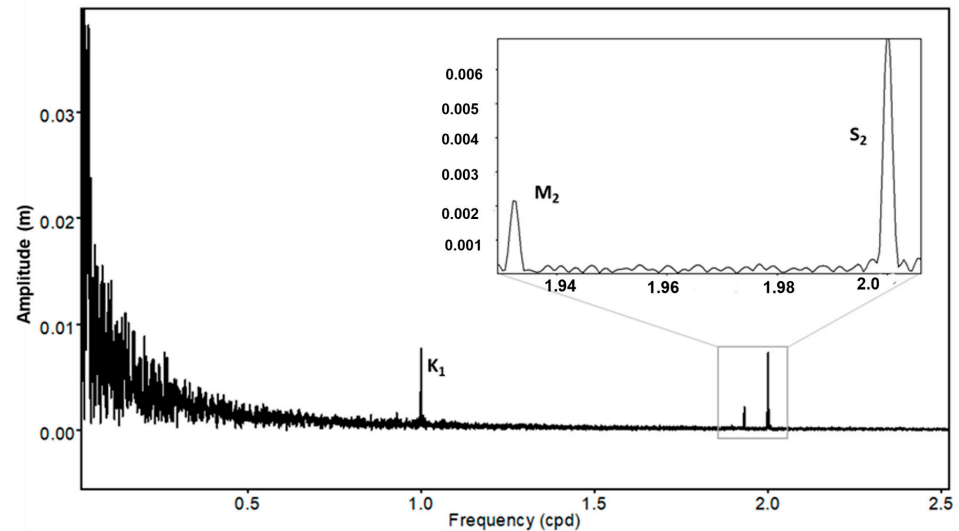


Figure 5. Amplitude spectra of harmonic frequencies, cpd (cycles per day) obtained from Fourier transformation of the groundwater level at borehole MH2 (Major tidal components are labelled on the periodogram).

The computed groundwater level spectra for borehole Z12836 show O_1 , K_1 , N_2 , M_2 and S_2 tidal constituents and indicate excellent tidal responses (Figure 6). The spectrum of the groundwater level indicates that fluctuations in the groundwater level in the boreholes occur at the same frequency as fluctuations in the pressure head in the aquifer induced by the Earth tides [49]. The N_2 component is small, and shows at a slightly lower frequency than the M_2 component (Figure 6). Groundwater level data associated with inland wells show the presence of the lunar harmonics O_1 and M_2 representing the effect of Earth tides, as the influence of ocean tides should be negligible and lunar harmonics do not have periodic oscillations in atmospheric pressure [57]. At a frequency of 1.9324 cpd corresponding to the M_2 tidal component, only Earth tide influences are present [48].

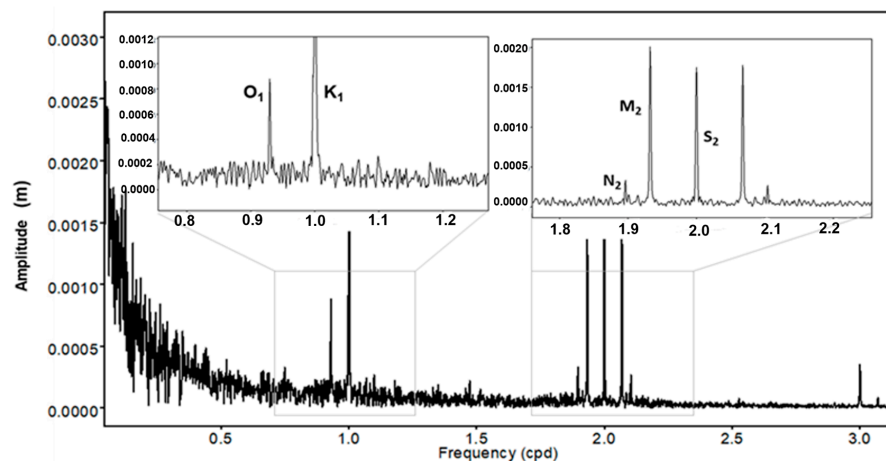


Figure 6. Amplitude spectra of harmonic frequencies, cpd (cycles per day) obtained from Fourier transformation of the groundwater level at borehole Z12836 (Major tidal components are labelled on the periodogram).

Clear atmospheric tidal harmonics at 1 cpd (S_1) constituent are shown by the barometric pressure spectra, which occur at the same harmonic frequency as the K_1 observed in the barometric spectra in Figure 7 [9,10,48]. The atmospheric harmonic S_1 can therefore interfere with the water level tidal reaction at this frequency [58]. Therefore, to estimate the hydrogeological properties, this study uses the stable M_2 constituent, which is present in the groundwater level spectrum of the two boreholes (MH2 and Z12836), as it is less affected by barometric pressure loading contamination [55].

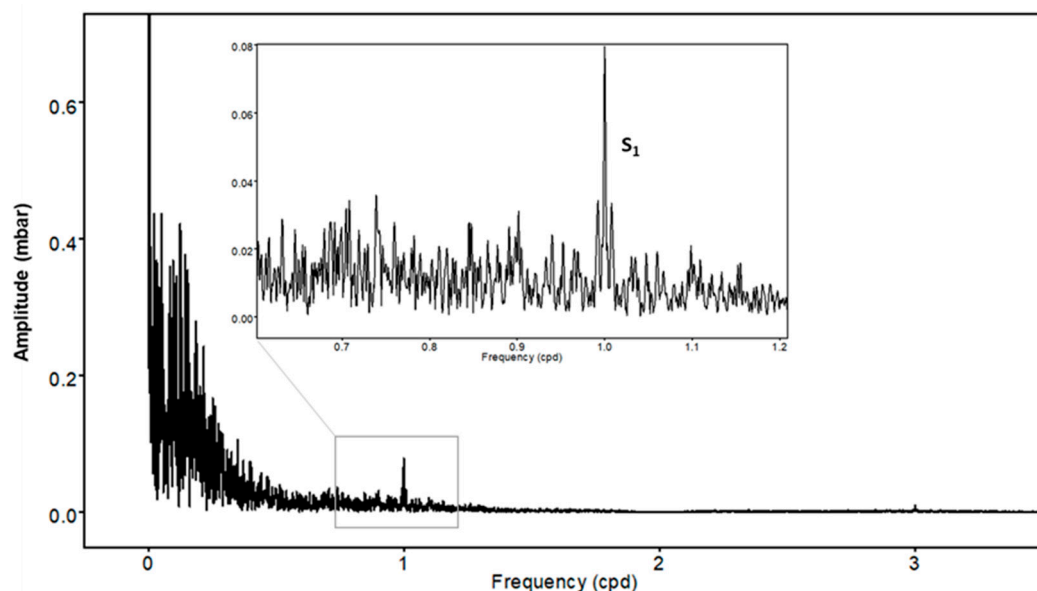


Figure 7. Amplitude spectra of harmonic frequencies, cpd (cycles per day) obtained from Fourier transformation of the barometric pressure at borehole BH7435 (Major tidal components are labelled on the periodogram).

3.3. Tidal Analysis

Seismic waves often change the permeability and storage properties of an aquifer system. Therefore, these properties can be estimated from the amplitude responses and phase shifts of tidal components of the groundwater level [8,15,64]. Thus, temporal variations in the tidal constants might reflect changes in aquifer hydraulic properties. In order to investigate potential earthquake-related temporal variation in hydraulic parameters, we measured the variability in amplitude and phase changes in groundwater level fluctuation relative to the M_2 tidal constituent's volumetric strain. Hsieh et al. [9] indicated that the earthquake-induced changes in transmissivity and storage coefficient can cause phase shift and amplitude variations of the tidal constituents.

The tidal amplitude and phase variation in the groundwater level to Earth tides for borehole MH2 are illustrated in Figure 8. The tidal amplitude ranged from 1.5 mm to 3.5 mm for borehole MH2 (Figure 8a). The observed amplitude response is constant without major variations, indicating that the aquifer's storage properties are constant and display no substantial changes [58]. The amplitude did not show major deviations except for April 2017, when the Moiyabana earthquake took place. The Moiyabana earthquake greatly enhanced the amplitude response of the groundwater level for borehole MH2. The tidal constants remained stable after the earthquake's occurrence. However, the changes in amplitude can be attributed to changes in storativity of the aquifer [8,9]. The amplitude variation of the M_2 was very small, which might be an indication that the storativity of the aquifer did not change significantly except after the Moiyabana earthquake.

The phase lag obtained from the tidal response of the groundwater level ranged from 75° to 117° and for borehole MH2 (Figure 8b) over the period considered (January 2016–December 2018) in this study with no major deviations. The positive and negative

phase shifts indicate the groundwater level advancing or lagging behind the tidal strain, respectively [10]. The computed t phase shift of the groundwater level for the M_2 tidal constituent in boreholes MH2 were both significantly changed by the Moiyabana earthquake (Figure 8b). The phase shift change from 10.592° to -3.434° after the earthquake took place, as observed in borehole MH2 (Figure 8b), may be indicating a decrease in the permeability of the aquifer.

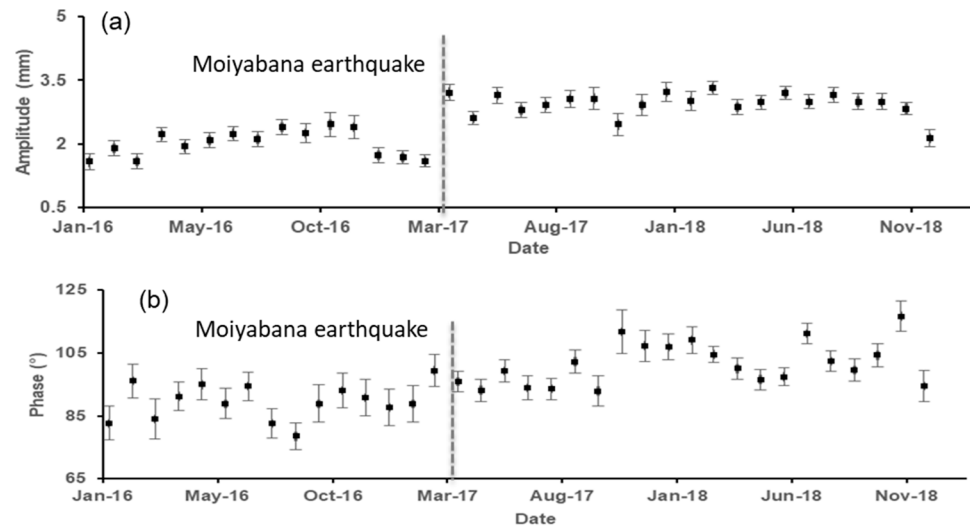


Figure 8. (a) Tidal amplitude variation, and (b) phase variation measured every 31 days at borehole MH2. Error bars indicate the root-mean-square error (RMSE) of the tidal analysis.

For borehole Z12836, the phase shift changed from -2.933° to positive 12.363° after the earthquake’s occurrence, suggesting that the permeability of the well-aquifer system may have been enhanced by the seismic waves (Figure 9). Phase shift changes have been documented to reflect changes in the aquifer permeability due to unclogging of pre-existing cracks by seismic waves [8]. In a confined aquifer, small phase lags are due to high permeability, while large phase lags are due to low permeability [11]. Thus, an increase in phase shift implies an increase in permeability [8,9]. However, the changes in amplitude can be attributed to changes in storativity of the aquifer [8,9]. After the Moiyabana earthquake, the amplitude ratio and phase shift remained constant, which may suggest that the hydraulic property changes caused by the earthquake at borehole Z12836 had not recovered [8,65] by the end of the analysed time span in this study.

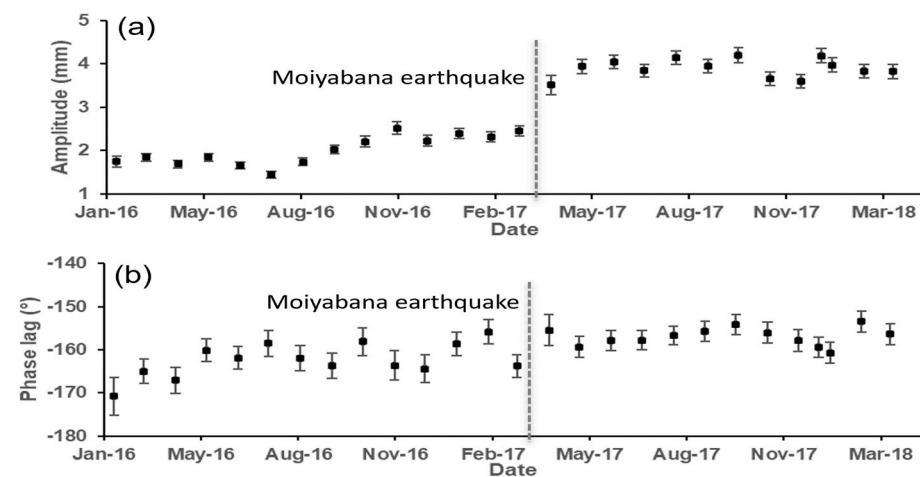


Figure 9. (a) Tidal amplitude variation, and (b) phase variation measured every 31 days at borehole Z12836. Error bars indicate the root-mean-square error (RMSE) of the tidal analysis.

These results are consistent with previous studies [2,6,8], which demonstrate that far-field earthquakes can enhance the aquifer permeability. The results of [2] showed that both the amplitude of the tidal response and the phase shift of the M_2 constituent increased, and that the post-earthquake phase shift changed from negative to positive and an increased in permeability was observed in the aquifer. In [8], characteristic M_2 wave co-seismic and post-seismic phase shifts observed in the wells in California suggested an enhancement of the aquifer's permeability as a potential cause for the phase shifts. Therefore, permeability enhancement following an earthquake event may be related to propagation of seismic waves.

Previous studies indicated that by analysing the tidal phase and amplitude ratio of the tidal constituents, the effect of enhanced horizontal permeability and increased vertical permeability could be distinguished [2,9,54,58]. A substantial change in the phase shift, along with in decreased amplitude ratio, suggests an enhancement of both the horizontal and vertical permeability [59]. However, the results of the tidal analysis of the Z12836 borehole showed a substantial increase in the phase shift (-2.933° to 12.363°) but a fairly small increase in the amplitude ratio (0.07614 to 0.10879) following the Moiyabana earthquake. A significant increase in the phase shift and small changes in the amplitude ratio can also imply a bidirectional increase in permeability [2,58].

The tidal analysis summary and the estimated hydraulic properties of the Ntane sandstone aquifer at boreholes MH2 and Z12836 before and after the earthquake are shown in Table 4. The temporal variations in transmissivity are interpreted as variations in permeability for the duration considered in this study as the aquifer thickness and fluid properties are unlikely to differ. The storativity of borehole MH2 decreased with a magnitude of 3.17432×10^{-4} after the earthquake. The transmissivity and permeability of borehole MH2 showed a decrease with a magnitude of 0.5609×10^{-5} m/s and 0.185 m²/day, respectively. The storativity decreased with a magnitude of 2.85×10^{-4} while the permeability was enhanced by 0.047 m² after the Moiyabana earthquake occurrence for borehole Z12836.

Table 4. Summary of the M_2 wave tidal and well-aquifer system hydraulic parameters for borehole. MH2 and Z12836 before and after the earthquake occurrence.

BH ID	Date	Tidal Amplitude (mm)	Phase Shift (°)	Specific Storage Ss (10^{-6} m^{-1})	Storativity (Dimensionless) S (10^{-4})	Transmissivity T ($10^{-5} \text{ m}^2/\text{s}$)	Permeability k (10^{-13} m^2)
MH2	Mar 17	1.592	10.592	20.172	6.25332	9.7766	3.215
	Apr 17	3.209	-3.437	9.933	3.079	9.2157	3.03
	Δ	1.617	-14.029	-10.521	-3.17432	-0.5609	-0.185
Z12836	Mar 17	2.46	-2.933	12.883	8.89	8.0638	1.191
	Apr 17	3.514	12.363	8.752	6.04	8.3799	1.238
	Δ	1.054	15.259	-4.131	-2.85	0.3161	0.047

4. Discussion

The storativity values (Table 4) obtained by the method of tidal analysis are consistent with the values obtained from the pumping test. A constant discharge rate aquifer test analysis resulted in a storativity of 1×10^{-4} and 2×10^{-4} for boreholes MH2 and Z12836, respectively, using the Cooper-Jacob analysis method. These values are within reasonable ranges of storativity for confined aquifers i.e., 0.5×10^{-5} to 5×10^{-3} [61,66]. Obtaining specific storage estimates within the same order of magnitude as the tidal analysis approach is satisfactory and the findings are consistent with the pumping test results.

The transmissivity estimate for borehole MH2 from the pumping test and tidal analysis were 6.822 m²/day and 8.44 m²/ day, respectively. This indicates that the transmissivity estimate from the tidal analysis method is within an acceptable range and is consistent with the constant rate test result, despite minor deviations. Although the scale of the region sampled by the tidal response is small, the pumping test and the tidal response yield a similar order of magnitude of permeability values. This might be an indication that within

the volume investigated by tides, the wells are efficiently interconnected with the fracture network [10].

For borehole Z12836 the constant rate test yielded a transmissivity and permeability of $3.9 \times 10^{-4} \text{ m}^2/\text{s}$ and $5.899 \times 10^{-13} \text{ m}^2$, respectively. The distinction in the obtained estimates of the transmissivity and permeability using the tidal analysis and pumping test could be that pumping test results are affected by the average properties inside the effective radius of the borehole. Therefore, presence of secondary fissures could result in higher hydraulic conductivity values estimates from pump test data analyses [67]. However, for a well-aquifer system that responds to tidal strain, the wells may not efficiently interconnect with the fracture network, which leads to lower transmissivity estimates. Thus, the estimated tidal analysis transmissivity values of borehole Z12836 are slightly lower than the pumping test values by an order of a magnitude.

The estimated permeability values from the tidal analysis are slightly lower than the permeability values from the pumping test estimates due to the influence of a larger skin effect in the tidal response method [58]. The higher initial displacement of the well water level during a pumping test can disrupt the skin effect; thus, a lower skin effect during the pumping test would result in a higher transmissivity value [10,58,68]. Although there is a slight difference in permeability estimates from the two methods, the difference is within a reasonable range. The target aquifer is often not fully confined (semi-confined) therefore it may be characterized by vertical leakage of the confining aquitard, which appears to result in a smaller amplitude ratio and a larger phase advance or a smaller phase lag in the aquifer below the aquitard [68]. An aquitard breach during seismic wave propagation can also cause vertical leakage. The pumping test and the tidal response yield similar permeability values, despite the smaller scale of the region sampled by the tidal response. This indicates that the wells are efficiently interconnected to the fracture network within the volume investigated using Earth tide response [10].

The sampling scale of a pumping test is the distance between the monitoring well and the pumping well [10]. Tidal responses are susceptible to scales ranging from one to tens of meters that are difficult to achieve with traditional methods such as pumping and slug tests [13]. The tidal process averages the properties of aquifers extending an effective radius of the order of $\sqrt{D\tau}$ from the well [8,58], where D (the transmissivity to storativity ratio) is the hydraulic diffusivity and τ is the tidal period. The approximate values evaluated around borehole MH2 using the tidal responses are in the range from 63 to 78 m and from 58 to 65 m for boreholes MH2 and Z12836, respectively, indicating that the scales of the values based on tidal response are similar to those of the pumping tests. However, larger-scale tests such as pumping tests in fractured-rock aquifers can capture more interconnected zones of fractures and preferential flow paths, which translate into higher transmissivity values [69].

Ground shaking caused by an earthquake may lead to the re-arrangement of solid grains, thus compacting them [70]. As borehole MH2 is located in the intermediate field, the strong ground shaking experienced might have contributed to the consolidation of the aquifer material and a resultant decrease in permeability. Volumetric changes in the rock mass in the near field cause pore pressure changes, thereby causing abrupt groundwater level increase in the nearby wells [71]. Increases in the groundwater level may also result from undrained dilatation or consolidation of sediments caused by strong ground shaking near the earthquake hypocentre. Decreases in groundwater level may be a sign of dilatancy related to fracture formation near the rupture fault [72].

The enhanced aquifer permeability at borehole Z12836 by the Moiyabana earthquake might be due to fracturing of the aquifer material [2,4,8,16,71]. We can infer that fractures which were blocked by colloids before the earthquake were unclogged as there was sufficient seismic energy for groundwater flow which drove colloids away from the fracture. This might lead to an increase in permeability after the seismic wave propagation [8,16]. In addition, fracture clearing and increased permeability due to the consolidation of loose sediments caused by the earthquake-induced dynamic stress have been widely used to ex-

plain most far-field water-level changes [2,8]. Dynamic shaking can also enhance effective permeability, especially that of fractured systems [8].

The groundwater levels of borehole Z12836 could not recover to the pre-earthquake water levels (after the Mw 6.5 Moiyabana earthquake); this suggests an increased groundwater discharge possibly through fractures generated or enhanced by the earthquake [3,6]. Seismic shaking is known to cause fracturing of the aquifer, and thus increasing groundwater outflow through the fractures would reduce pore pressure. Consequently, the aquifer in the long run cannot return to the original state [3].

5. Conclusions

The Mw 6.5 Moiyabana earthquake significantly affected the groundwater levels in borehole MH2 and Z12836 and subsequently the hydraulic properties of the Ntane sandstone aquifer. The storativity of the Ntane sandstone aquifer around borehole MH2 and Z12836 decreased after the Mw 6.5 Moiyabana earthquake. Following the earthquake's occurrence, the permeability was decreased at borehole MH2, while at borehole Z12836, the permeability of the aquifer was enhanced. Changes in aquifer permeability may have a major effect on groundwater flow, and therefore on groundwater sources and the potential for solute transport may increase; thus, they can be useful in evaluating groundwater resources and solute transport in tectonically active areas. From this study, we can conclude that the tidal analysis of the groundwater levels can be used for reliable and accurate estimation of the aquifer's properties and for determining their temporal variation.

Author Contributions: Conceptualization, T.M.M., L.M. and E.M.S.; methodology, T.M.M. and L.M.; data analysis, T.M.M.; data sourcing, E.M.S.; writing—original draft preparation, T.M.M.; writing—review and editing, L.M. and E.M.S.; supervision, L.M. and E.M.S. All authors have read and agreed to the published version of the manuscript.

Funding: This research is part of an MSc thesis by T.M.M., partially funded by Botswana International University of Science and Technology, grant number S00162.

Data Availability Statement: 3rd Party Data; Restrictions apply to the availability of these data. Data were obtained from Department of Water & Sanitation, Ghaghoo Diamond Mine and CIC Energy and are available from the corresponding author with permission from the listed parties.

Acknowledgments: The authors would like to extend their gratitude to the Department of Water & Sanitation (DWS), Ghaghoo Diamond mine and CIC Energy for allowing them to use the data for this research, Yuichi Kitagawa for assisting with Baytap-G, Phemelo Makoba and Moiteela Lekula for data sourcing at DWS.

Conflicts of Interest: The authors declare that they have no conflict of interest and no prior publication of the work reported in this paper.

References

1. Lee, J.M.; Woo, N.C.; Koh, D.-C.; Kim, K.-Y.; Ko, K.-S. Assessing aquifer responses to earthquakes using temporal variations in groundwater monitoring data in alluvial and sedimentary bedrock aquifers. *Geomat. Nat. Hazards Risk* **2020**, *11*, 742–765. [[CrossRef](#)]
2. Zhang, S.; Shi, Z.; Wang, G. Comparison of aquifer parameters inferred from water level changes induced by slug test, earth tide and earthquake—A case study in the three Gorges area. *J. Hydrol.* **2019**, *579*, 124169. [[CrossRef](#)]
3. Liu, C.-Y.; Chia, Y.; Chuang, P.-Y.; Chiu, Y.-C.; Tseng, T.-L. Impacts of hydrogeological characteristics on groundwater-level changes induced by earthquakes. *Hydrogeol. J.* **2017**, *26*, 451–465. [[CrossRef](#)]
4. Wang, C.Y.; Manga, M. Hydrologic responses to earthquakes and a general metric. *Geofluids* **2010**, *10*, 206–216.
5. Wang, C.-H.; Kuo, C.-H. Temporal change in groundwater level following the 1999 (Mw = 7.5) Chi-Chi earthquake, Taiwan. *Geofluids* **2004**, *4*, 210–220. [[CrossRef](#)]
6. Sun, X.; Wang, G.; Yang, X. Coseismic response of water level in Changping well, China, to the Mw 9.0 Tohoku earthquake. *J. Hydrol.* **2015**, *531*, 1028–1039. [[CrossRef](#)]
7. Roeloffs, A. Persistent water level changes in a well near Parkfield, California, due to local and distant earthquakes. *J. Geophys. Res.* **1998**, *103*, 869–889. [[CrossRef](#)]
8. ElKhoury, J.E.; Brodsky, E.E.; Agnew, D.C. Seismic waves increase permeability. *Nature* **2006**, *441*, 1135–1138. [[CrossRef](#)]

9. Hsieh, P.A.; Bredehoeft, J.D.; Farr, J.M. Determination of aquifer transmissivity from Earth tide analysis. *Water Resour. Res.* **1987**, *23*, 1824–1832. [[CrossRef](#)]
10. Allègre, V.; Brodsky, E.E.; Xue, L.; Nale, S.M.; Parker, B.L.; Cherry, J.A. Using earth-tide induced water pressure changes to measure in situ permeability: A comparison with long-term pumping tests. *Water Resour. Res.* **2016**, *52*, 3113–3126. [[CrossRef](#)]
11. Zhang, Y.; Fu, L.-Y.; Ma, Y.; Hu, J. Different hydraulic responses to the 2008 Wenchuan and 2011 Tohoku earthquakes in two adjacent far-field wells: The effect of shales on aquifer lithology. *Earth Planets Space* **2016**, *68*, 178. [[CrossRef](#)]
12. Bredehoeft, J.D. United States. Geological Survey WD. Response of well-aquifer systems to Earth tides. *J. Geophys. Res. Atmos.* **1967**, *72*, 3075–3087. [[CrossRef](#)]
13. Hsieh, P.A.; Bredehoeft, J.D.; Rojstaczer, S.A. Response of well aquifer systems to Earth tides: Problem revisited. *Water Resour. Res.* **1988**, *24*, 468–472. [[CrossRef](#)]
14. Rojstaczer, S.; Agnew, D. The influence of formation material properties on the response of water levels in wells to Earth tides and atmospheric loading. *J. Geophys. Res. Atmos.* **1989**, *94*, 12403–12411. [[CrossRef](#)]
15. Matsumoto, N.; Roeloffs, E.A. Hydrological response to earthquakes in the Haibara well, central Japan-II. Possible mechanism inferred from time-varying hydraulic properties. *Geophys. J. Int.* **2003**, *155*, 899–913. [[CrossRef](#)]
16. Brodsky, E.E.; Roeloffs, E.; Woodcock, D.; Gall, I.; Manga, M. A mechanism for sustained groundwater pressure changes induced by distant earthquakes. *J. Geophys. Res. Atmos.* **2003**, *108*, B8. [[CrossRef](#)]
17. Montgomery, D.R.; Greenberg, H.M.; Smith, D.T. Streamflow response to the Nisqually earthquake. *Earth Planet. Sci. Lett.* **2003**, *209*, 19–28. [[CrossRef](#)]
18. Lai, G.; Jiang, C.; Han, L.; Sheng, S.; Ma, Y. Co-seismic water level changes in response to multiple large earthquakes at the LGH well in Sichuan, China. *Tectonophysics* **2016**, *679*, 211–217. [[CrossRef](#)]
19. Shi, Z.; Wang, G.; Manga, M.; Wang, C.Y. Mechanism of co-seismic water level change following four great earthquakes—Insights from co-seismic responses throughout the Chinese mainland. *Earth Planet. Sci. Lett.* **2015**, *430*, 66–74. [[CrossRef](#)]
20. Xue, L.; Li, H.-B.; Brodsky, E.E.; Xu, Z.-Q.; Kano, Y.; Wang, H.; Mori, J.J.; Si, J.-L.; Pei, J.-L.; Zhang, W.; et al. Continuous Permeability Measurements Record Healing inside the Wenchuan Earthquake Fault Zone. *Science* **2013**, *340*, 1555–1559. [[CrossRef](#)]
21. Liao, X.; Wang, C.-Y.; Liu, C.-P. Disruption of groundwater systems by earthquakes. *Geophys. Res. Lett.* **2015**, *42*, 9758–9763. [[CrossRef](#)]
22. Kolawole, F.; Atekwana, E.A.; Malloy, S.; Stamps, D.S.; Grandin, R.; Abdelsalam, M.G.; Leseane, K.; Shemang, E.M. Aeromagnetic, gravity, and Differential Interferometric Synthetic Aperture Radar analyses reveal the causative fault of the 3 April 2017 Mw 6.5 Moiyabana, Botswana, earthquake. *Geophys. Res. Lett.* **2017**, *44*, 8837–8846. [[CrossRef](#)]
23. Midzi, V.; Saunders, I.; Manzunzu, B.; Kwadiba, M.; Jele, V.; Mantsha, R.; Marimira, K.; Mulabisana, T.; Ntibinyane, O.; Pule, T.; et al. The 03 April 2017 Botswana M6.5 earthquake: Preliminary results. *J. Afr. Earth Sci.* **2018**, *143*, 187–194. [[CrossRef](#)]
24. Modisi, M.P.; Atekwana, E.A.; Kampunzu, A.B.; Ngwisanyi, T.H. Rift kinematics during the incipient stages of continental extension: Evidence the nascent Okavango rift basin, Northwest Botswana. *Geology* **2000**, *28*, 939–942. [[CrossRef](#)]
25. Simon, R.E.; Kwadiba, M.T.O.; King, J.G.; Moidaki, M. A History of Botswana’s Seismic Network. *Botsw. Notes Rec.* **2012**, *44*, 184–192. Available online: <http://www.jstor.com/stable/43> (accessed on 28 February 2018).
26. Albano, M.; Polcari, M.; Bignami, C.; Moro, M.; Saroli, M.; Stramondo, S. Did Anthropogenic Activities Trigger the 3 April 2017 Mw 6.5 Botswana Earthquake? *Remote. Sens.* **2017**, *9*, 1028. [[CrossRef](#)]
27. Fadel, I.; van der Meijde, M.; Paulssen, H. Crustal Structure and Dynamics of Botswana. *J. Geophys. Res. Solid Earth* **2018**, *123*, 10659–10671. [[CrossRef](#)]
28. Gardonio, B.; Jolivet, R.; Calais, E.; Leclère, H. The April 2017 Mw 6.5 Botswana Earthquake: An Intraplate Event Triggered by Deep Fluids. *Geophys. Res. Lett.* **2018**, *45*, 8886–8896. [[CrossRef](#)]
29. Moorkamp, M.; Fishwick, S.; Walker, R.J.; Jones, A.G. Geophysical evidence for crustal and mantle weak zones controlling intra-plate seismicity—The 2017 Botswana earthquake sequence. *Earth Planet. Sci. Lett.* **2018**, *506*, 175–183. [[CrossRef](#)]
30. Lekula, M.; Lubczynski, M.W.; Shemang, E.M. Hydrogeological conceptual model of large and complex sedimentary aquifer systems—Central Kalahari Basin. *Phys. Chem. Earth Parts A/B/C* **2018**, *106*, 47–62. [[CrossRef](#)]
31. Smith, R. The Lithostratigraphy of the Karoo Supergroup in Botswana. Bulletin 2. Department of Geological Survey. *Bull.-Geol. Surv. Dep. Repub. Botswana*. **1984**, *26*, 239.
32. Williamson, L.; District, M. The geology of the area around Mmamabula and Dibete: Including an account of the Greater Mmamabula Coalfield. *Dep. Geol. Surv.* **1996**, *6*, 40–105.
33. Carney, J.; Aldiss, D.; Lock, N. *The Geology of Botswana, Bulletin37*; Bulletin37 1st ed.; Department of Geological Survey: Gaborone, Botswana, 1994.
34. Reeves, C.; Hutchins, D. A progress report on the geophysical exploration of the Kalahari in Botswana. *Geoexploration* **1982**, *20*, 209–224. [[CrossRef](#)]
35. Hutchins, D.; Reeves, C. Regional geophysical exploration of the Kalahari in Botswana. *Tectonophysics* **1980**, *69*, 201–220. [[CrossRef](#)]
36. Chisenga, C.; Van der Meijde, M.; Yan, J.; Fadel, I.; Atekwana, E.A.; Steffen, R.; Ramotoroko, C. Gravity derived crustal thickness model of Botswana: Its implication for the Mw 6.5 April 3, 2017, Botswana earthquake. *Tectonophysics* **2020**, *787*, 228479. [[CrossRef](#)]
37. Rajesh, H.; Safonov, O.; Basupi, T.; Belyanin, G.; Tsunogae, T. Complexity of characterizing granitoids in high-grade terranes: An example from the Neoproterozoic Verbaard granitoid, Limpopo Complex, Southern Africa. *Lithos* **2018**, *318–319*, 399–418. [[CrossRef](#)]

38. Obakeng, O.T.; de Vries, J.J.; Lubczynski, M.W. *Soil Moisture Dynamics and Evapotranspiration at the Fringe of the Botswana Kalahari, with Emphasis on Deep Rooting Vegetation*; Vrije Universiteit: Amsterdam, The Netherlands, 2007.
39. Nthaba, B.; Simon, R.E.; Ogubazghi, G.M. Seismicity Study of Botswana from 1966 to 2012. *Int. J. Geosci.* **2018**, *9*, 707–718. [[CrossRef](#)]
40. SMEC; EHES. *Botswana National Water Master Plan Review*; Department of Water Affairs: Gaborone, Botswana, 2006; Volume 4.
41. WRC. Consultancy Services for the Post—Auditing of the Palla Road Groundwater Model (Palla Road & Chepete Wellfields) TENDER NO: MTC\MMEWR\DWA\1\29\11-12. Draft Modelling Report. Gaborone, Botswana, 2012.
42. WCS. *Kudumatse Block Groundwater Investigation—Borehole Z12836*; WCA: New York, NY, USA, 2007.
43. Van Biljon, M. *Geological Investigation and Groundwater Modelling at the Proposed Gope Diamond Mine Project*; Botswana, 2008.
44. Cooper, H.H., Jr.; Jacob, C.E. A generalized graphical method for evaluating formation constants and summarizing well-field history. *Eos, Transactions American Geophysical Union. Eos Trans. Am. Geophys. Union* **1946**, *27*, 526–534. [[CrossRef](#)]
45. Shi, Z.; Wang, G. Sustained groundwater level changes and permeability variation in a fault zone following the 12 May 2008, M_w 7.9 Wenchuan earthquake. *Hydrol. Process.* **2014**, *29*, 2659–2667. [[CrossRef](#)]
46. He, A.; Singh, R.P. Groundwater level response to the Wenchuan earthquake of May 2008. *Geomat. Nat. Hazards Risk* **2018**, *10*, 336–352. [[CrossRef](#)]
47. Van Camp, M.; Vauterin, P. Tsoft: Graphical and interactive software for the analysis of time series and Earth tides. *Comput. Geosci.* **2005**, *31*, 631–640. [[CrossRef](#)]
48. Acworth, R.L.; Halloran, L.J.S.; Rau, G.C.; Cuthbert, M.O.; Bernardi, T.L. An objective frequency domain method for quantifying confined aquifer compressible storage using Earth and atmospheric tides. *Geophys. Res. Lett.* **2016**, *43*, 11671–11678. [[CrossRef](#)]
49. Cuttillo, P.A.; Bredehoeft, J.D. Estimating Aquifer Properties from the Water Level Response to Earth Tides. *Groundwater* **2010**, *49*, 600–610. [[CrossRef](#)] [[PubMed](#)]
50. Fuentes-Arreazola, M.A.; Ramírez-Hernández, J.; Vázquez-González, R. Hydrogeological Properties Estimation from Groundwater Level Natural Fluctuations Analysis as a Low-Cost Tool for the Mexicali Valley Aquifer. *Water* **2018**, *10*, 586. [[CrossRef](#)]
51. Ishiguro, M.; Tamura, Y. BAYTAP-G in TIMSAC-84, in Computer Science Monographs. *Inst. Stat. Math.* **1985**, *22*, 56–117.
52. Tamura, Y.; Sato, T.; Ooe, M.; Ishiguro, M. A procedure for tidal analysis with a Bayesian information criterion. *Geophys. J. Int.* **1991**, *104*, 507–516. [[CrossRef](#)]
53. Munk, W.; MacDonald, G.J. *The Rotation of the Earth*; Cambridge University Press: London, UK, 1960; p. 68.
54. Roeloffs, E. Poroelastic Techniques in the Study of Earthquake-Related Hydrologic Phenomena. *Adv. Geophys.* **1996**, *37*, 135–195. [[CrossRef](#)]
55. Xue, L.; Brodsky, E.E.; Erskine, J.; Fulton, P.M.; Carter, R. A permeability and compliance contrast measured hydrogeologically on the San Andreas Fault. *Geochem. Geophys. Geosyst.* **2016**, *17*, 858–871. [[CrossRef](#)]
56. Marine, I.W. Water level fluctuations due to earth tides in a well pumping from slightly fractured crystalline rock. *Water Resour. Res.* **1975**, *11*, 165–173. [[CrossRef](#)]
57. Merritt, M. *Estimating Hydraulic Properties of the Floridan Aquifer System by Analysis of Earth-Tide, Ocean-Tide, and Barometric Effects, Collier and Hendry Counties, Florida*; US Department of the Interior; US Geological Survey: Reston, VA, USA, 2004.
58. Shen, Q.; Zheming, S.; Guangcai, W.; Qingyu, X.; Zejun, Z.; Jiaqian, H. Using water-level fluctuations in response to Earth-tide and barometric-pressure changes to measure the in-situ hydrogeological properties of an overburden aquifer in a coalfield. *Hydrogeol. J.* **2020**, *28*, 1465–1479. [[CrossRef](#)]
59. Wang, C.; Doan, M.; Xue, L.; Barbour, A.J. Tidal Response of Groundwater in a Leaky Aquifer—Application to Oklahoma. *Water Resour. Res.* **2018**, *54*, 8019–8033. [[CrossRef](#)]
60. Wang, H.F. *Theory of Linear Poroelasticity with Applications to Geomechanics and Hydrogeology*; Princeton University Press: Princeton, NJ, USA, 2001. [[CrossRef](#)]
61. Freeze, R.A.; Cherry, J.A. *Groundwater. Englewood Cliffs*; Prentice-Hall: Hoboken, NJ, USA, 1979.
62. Zhang, H.; Shi, Z.; Wang, G.; Sun, X.; Yan, R.; Liu, C. Large Earthquake Reshapes the Groundwater Flow System: Insight from the Water-Level Response to Earth Tides and Atmospheric Pressure in a Deep Well. *Water Resour. Res.* **2019**, *55*, 4207–4219. [[CrossRef](#)]
63. Zhang, S.; Shi, Z.; Wang, G.; Zhang, Z. Quantitative Assessment of the Mechanisms of Earthquake-Induced Groundwater-Level Change in the MP Well, Three Gorges Area. *Pure Appl. Geophys.* **2018**, *175*, 2475–2484. [[CrossRef](#)]
64. Shibata, T.; Takahashi, R.; Takahashi, H.; Kagoshima, T.; Takahata, N.; Sano, Y.; Pinti, D.L. Coseismic changes in groundwater level during the 2018 Hokkaido Eastern Iwate earthquake. *Earth Planets Space* **2020**, *72*, 23. [[CrossRef](#)]
65. Yan, R.; Wang, G.; Shi, Z. Sensitivity of hydraulic properties to dynamic strain within a fault damage zone. *J. Hydrol.* **2016**, *543*, 721–728. [[CrossRef](#)]
66. Fetter, C. *Applied Hydrogeology*, 4th ed.; Waveland Press: Salem, WI, USA, 2001; Volume 4.
67. Burbey, T.J.; Hisz, D.; Murdoch, L.C.; Zhang, M. Quantifying fractured crystalline-rock properties using well tests, earth tides and barometric effects. *J. Hydrol.* **2012**, *414–415*, 317–328. [[CrossRef](#)]
68. Gao, X.; Sato, K.; Horne, R.N. General Solution for Tidal Behavior in Confined and Semiconfined Aquifers Considering Skin and Wellbore Storage Effects. *Water Resour. Res.* **2020**, *56*, e2020WR027195. [[CrossRef](#)]
69. Kumar, T.J.R.; Balasubramanian, A.; Kumar, R.S.; Dushiyanthan, C.; Thiruneelakandan, B.; Suresh, R.; Karthikeyan, K.; Davidraju, D. Assessment of groundwater potential based on aquifer properties of hard rock terrain in the Chittar-Uppodai watershed, Tamil Nadu, India. *Appl. Water Sci.* **2014**, *6*, 179–186. [[CrossRef](#)]

70. Nespoli, M.; Todesco, M.; Serpelloni, E.; Belardinelli, M.E.; Bonafede, M.; Marcaccio, M.; Rinaldi, A.P.; Anderlini, L.; Gualandi, A. Modeling earthquake effects on groundwater levels: Evidences from the 2012 Emilia earthquake (Italy). *Geofluids* **2015**, *16*, 452–463. [[CrossRef](#)]
71. Wang, C.-Y.; Chia, Y. Mechanism of water level changes during earthquakes: Near field versus intermediate field. *Geophys. Res. Lett.* **2008**, *35*, L12402. [[CrossRef](#)]
72. Wang, C.-Y.; Manga, M.; Chen, C.-H. Transient change in groundwater temperature after earthquakes. *Geology* **2012**, *40*, 119–122. [[CrossRef](#)]

Disclaimer/Publisher’s Note: The statements, opinions and data contained in all publications are solely those of the individual author(s) and contributor(s) and not of MDPI and/or the editor(s). MDPI and/or the editor(s) disclaim responsibility for any injury to people or property resulting from any ideas, methods, instructions or products referred to in the content.